Supplementary Information

DFT Investigation of Active Sites in Metal-Doped Ferrierite Zeolites for Selective Methane Oxidation to Methanol

Zirong Guan[a,#], Jiaming Miao[a,#], Wenfu Yan[a], Zexing Qu[b,*], Yi Li[a,c,*]

[1]State Key Laboratory of Inorganic Synthesis and Preparative Chemistry, College of Chemistry, Jilin University, 2699 Qianjin Street, Changchun 130012, P. R. China

[2]Institute of Theoretical Chemistry, College of Chemistry, Jilin University, Changchun, 130023, P. R. China

[3]International Center of Future Science, Jilin University, Changchun 130012, P. R. China

*Corresponding Author(s):

zxqu@jlu.edu.cn

yili@jlu.edu.cn

Table of Contents for the Supplementary Information:

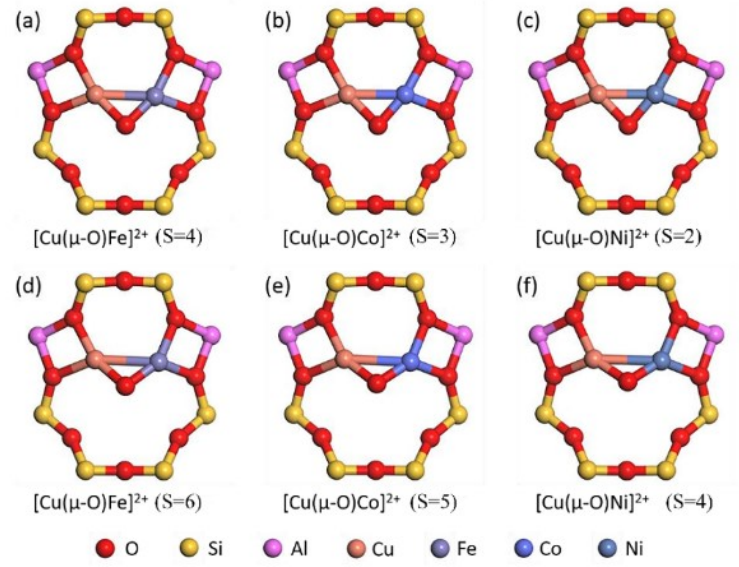

Figure S1 Geometry of $[Cu(\mu\text{-}O)M]^{2+}$-FER optimized at different spin multiplicities.

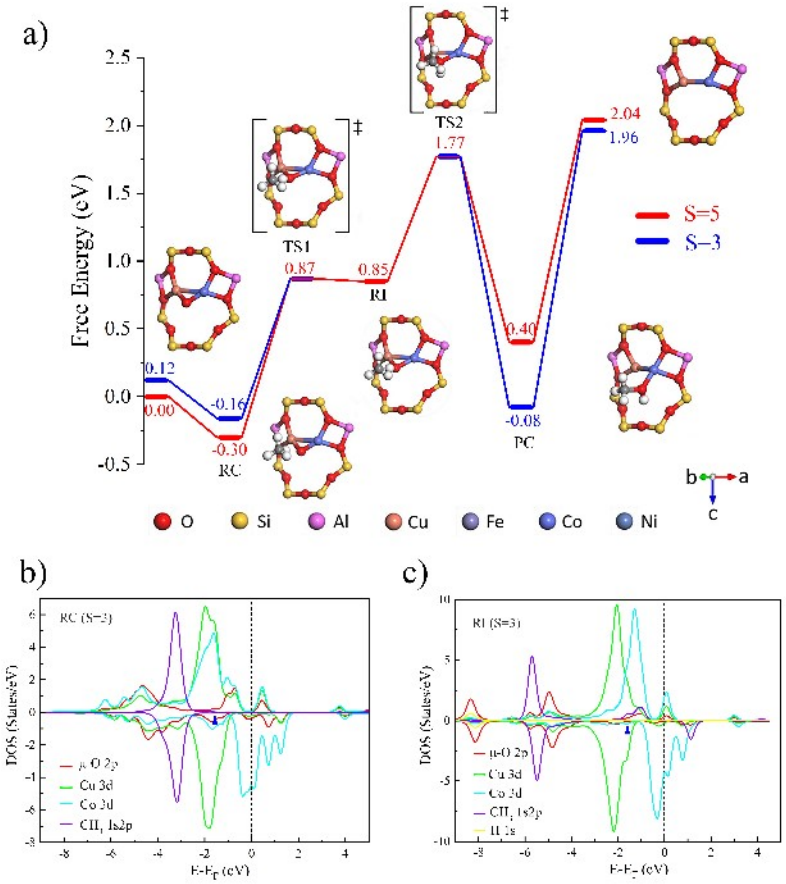

Figure S2 a) Free energy diagram of $[Cu(\mu\text{-}O)Co]^{2+}$-FER catalyzing CH_4 to CH_3OH at different multiplicities (red represents S=5, blue represents S=3). The PDOS of b) reactant complex and c) radical Intermediate (RI) catalyzed by $[Cu(\mu\text{-}O)Co]^{2+}$-FER. The d-band centers are pointed by arrows and listed in Table S5.

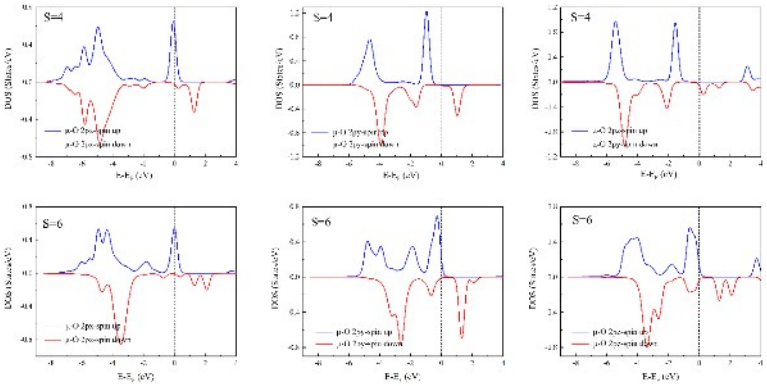

Figure S3 The PDOS diagram of 2p orbitals of μ-O in $[Cu(\mu\text{-}O)Fe]^{2+}$-FER with different spin multiplicities

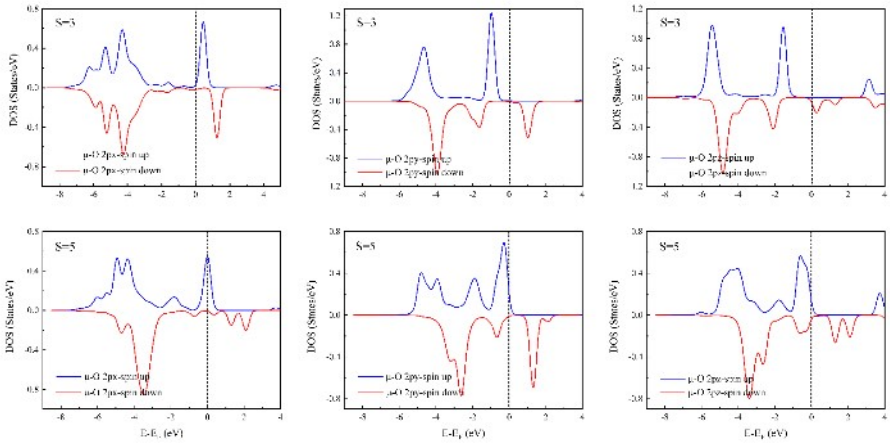

Figure S4 The PDOS diagram of 2p orbitals of μ-O in $[Cu(\mu\text{-}O)Co]^{2+}$-FER with different spin multiplicities

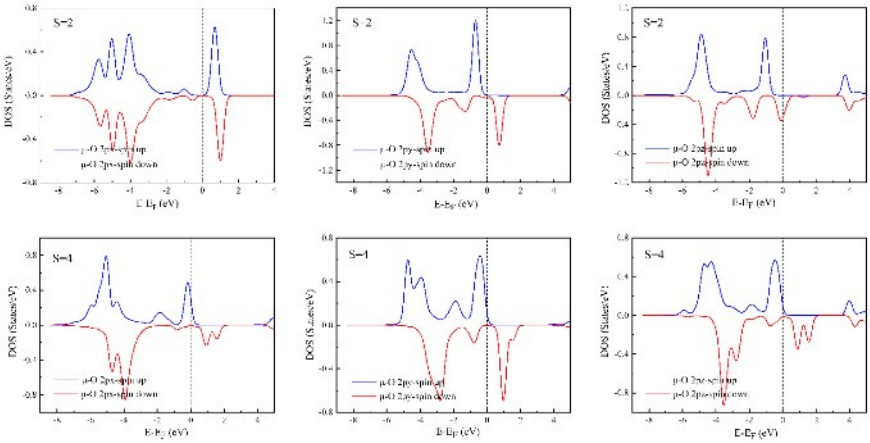

Figure S5 The PDOS diagram of 2p orbitals of μ-O in $[Cu(\mu\text{-}O)Ni]^{2+}$-FER with different spin multiplicities

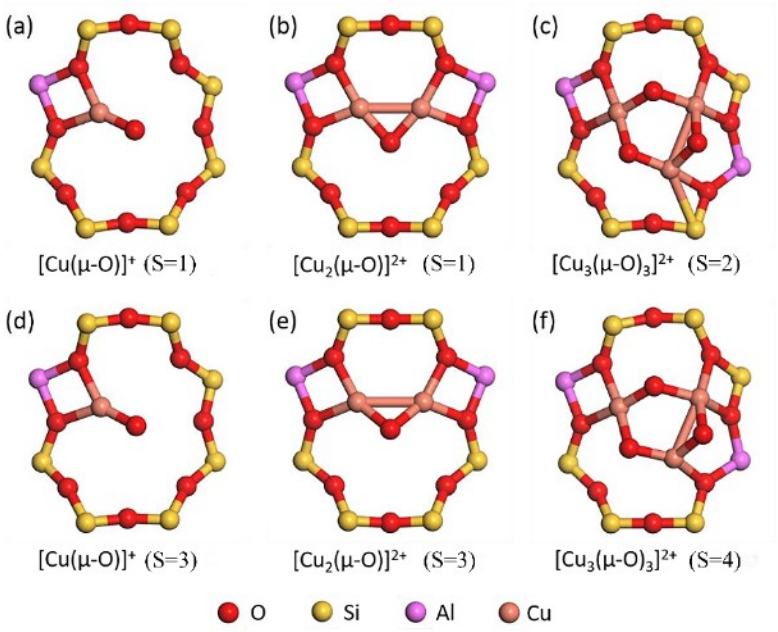

Figure S6 Geometry of $[Cu_x(\mu\text{-}O)_y]^{n+}$-FER optimized at different spin multiplicities

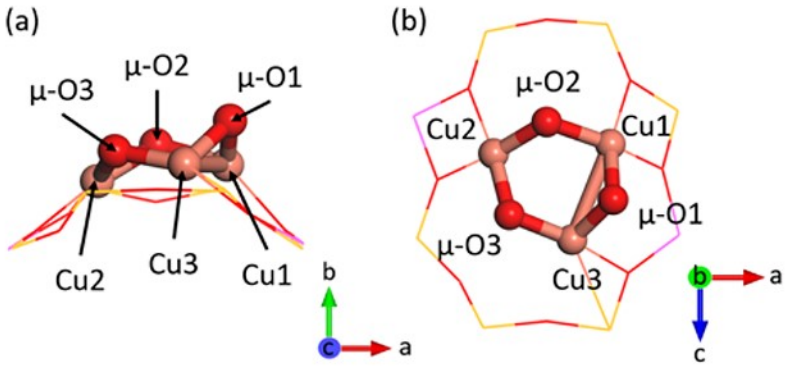

Figure S7 The diagrams of the corresponding numbers μ-O_1, μ-O_2, and μ-O_3 for the three bridged oxygen atoms of the $[Cu_3(\mu\text{-}O)_3]^{2+}$ active site, as well as the corresponding numbers Cu_1, Cu_2, and Cu_3 for the three copper atoms in this paper

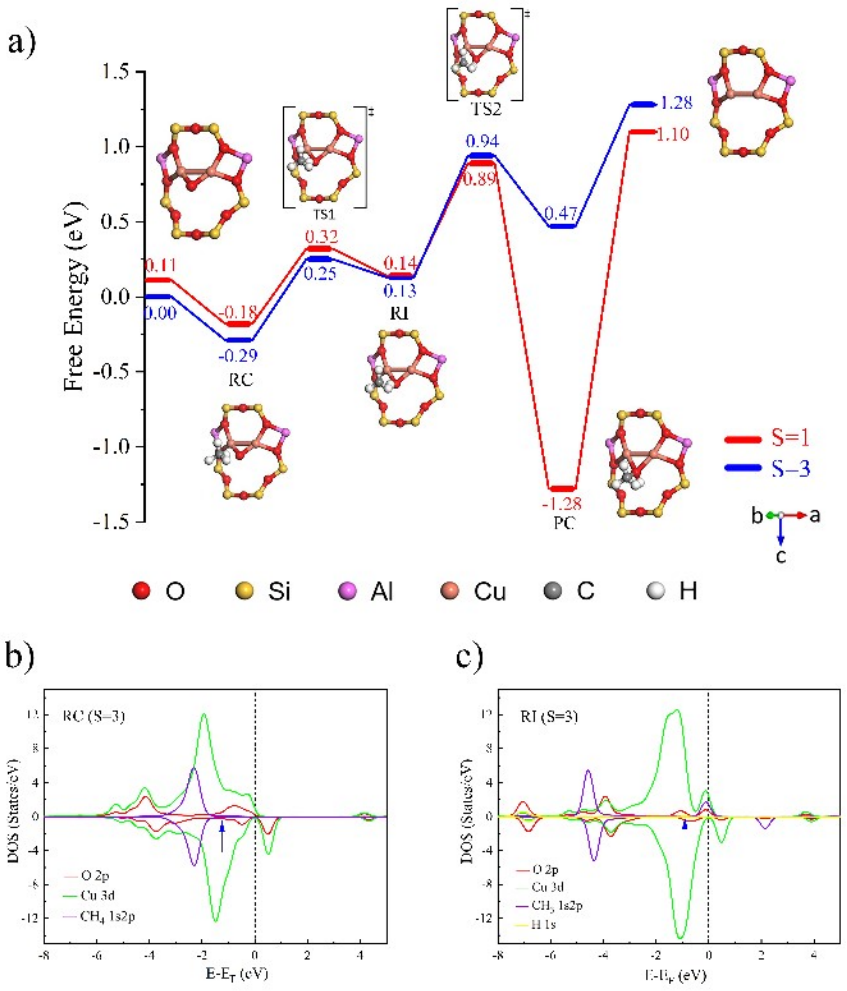

Figure S8 a) Free energy diagram of $[Cu_2(\mu\text{-}O)]^{2+}$-FER catalyzing CH_4 to CH_3OH at different multiplicities (red represents S=1, blue represents S=3). The PDOS of b) reactant complex and c) radical Intermediate (RI) catalyzed by $[Cu_2(\mu\text{-}O)]^{2+}$-FER. The d-band centers are pointed by arrows and listed in Table S15.

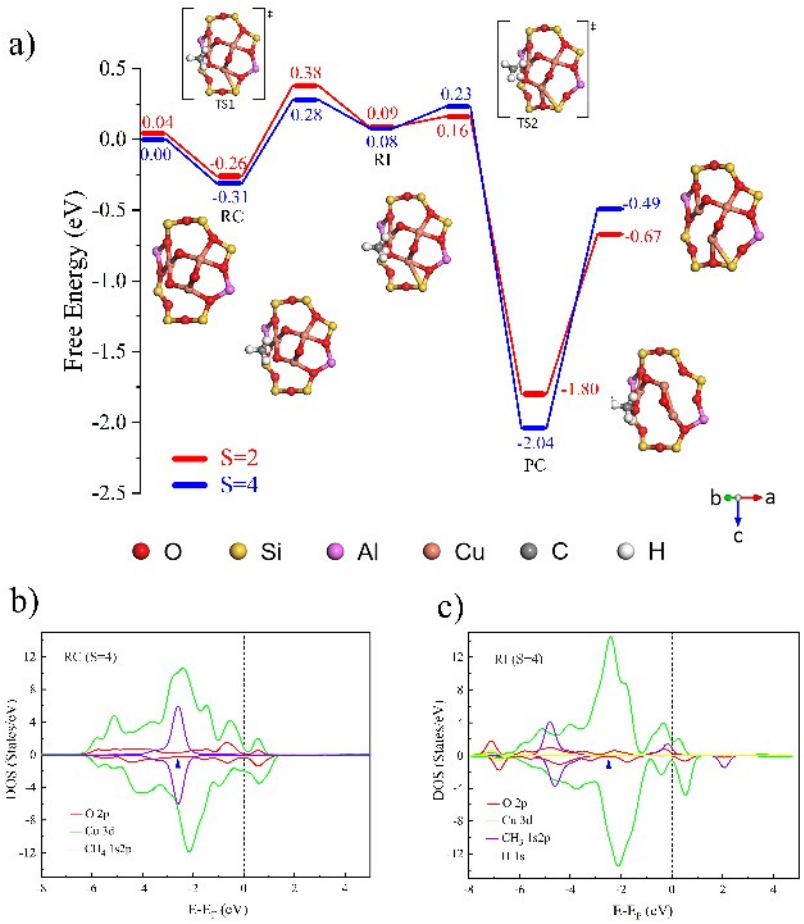

Figure S9 a) Free energy diagram of $[Cu_3(\mu\text{-}O)_3]^{2+}$-FER ($\mu\text{-}O_2$) catalyzing CH_4 to CH_3OH at different multiplicities (red represents S=2, blue represents S=4). The PDOS of b) reactant complex and c) radical Intermediate (RI) catalyzed by $[Cu_3(\mu\text{-}O)_3]^{2+}$-FER ($\mu\text{-}O_2$). The d-band centers are pointed by arrows and listed in Table S15.

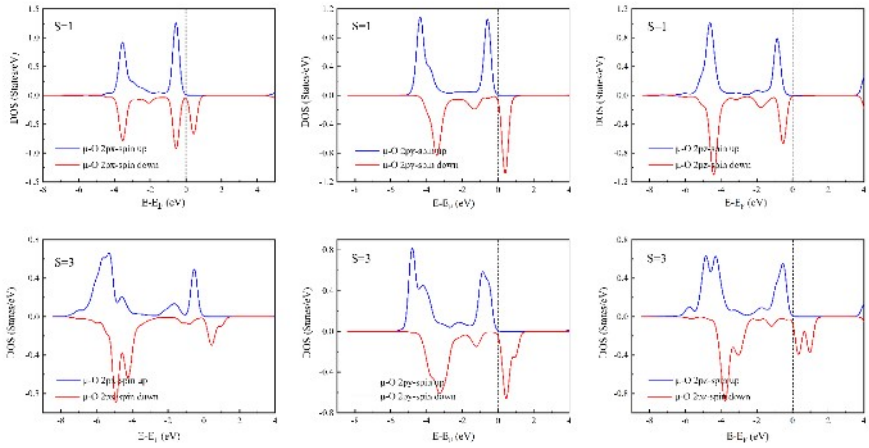

Figure S10 The PDOS diagram of 2p orbitals of μ-O in $[CuO]^+$-FER with different spin multiplicities

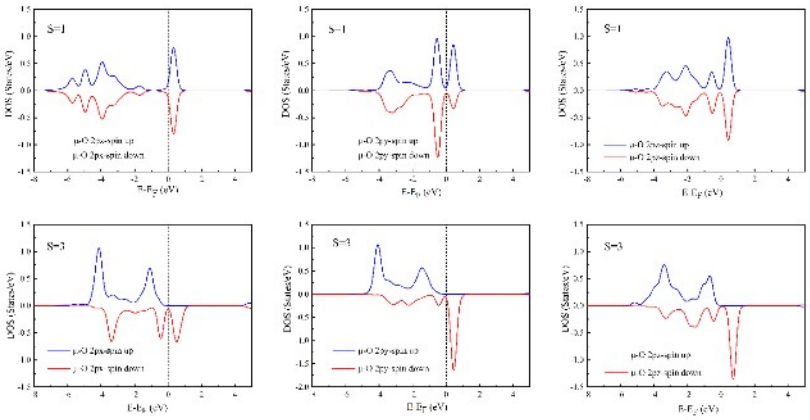

Figure S11 The PDOS diagram of 2p orbitals of μ-O in $[Cu_2(\mu\text{-}O)]^{2+}$-FER with different spin multiplicities

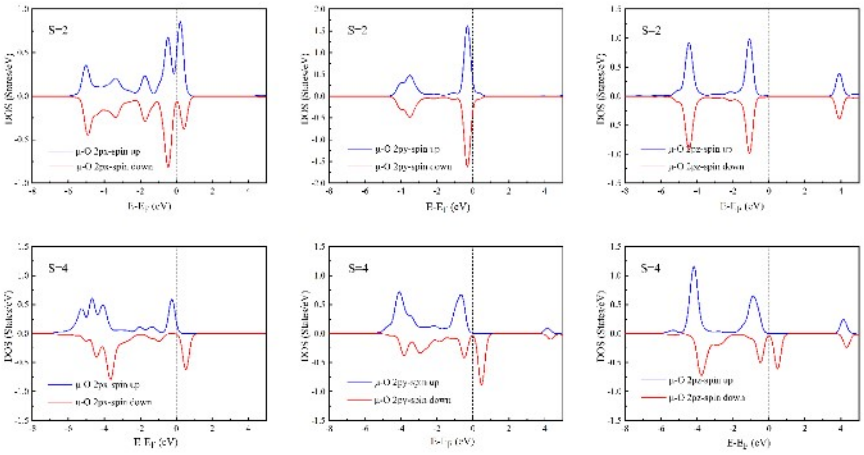

Figure S12 The PDOS diagram of 2p orbitals of μ-O in $[Cu_3(\mu\text{-}O)_3]^{2+}$-FER($\mu\text{-}O_1$) with different spin multiplicities

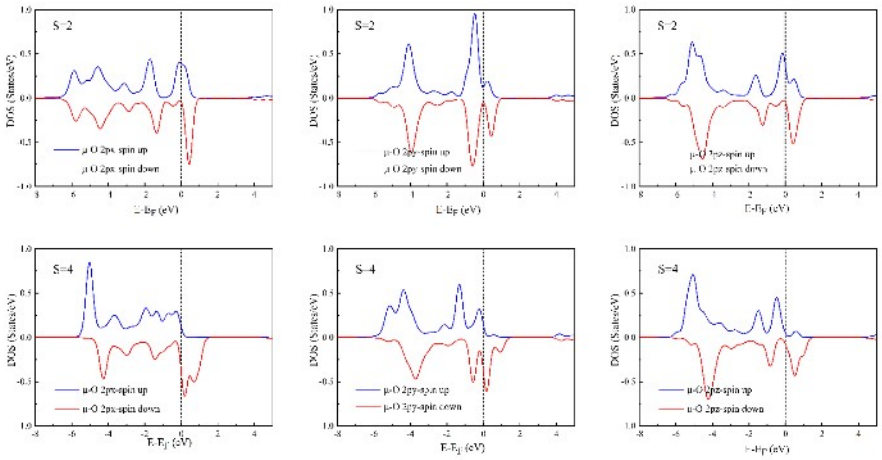

Figure S13 The PDOS diagram of 2p orbitals of μ-O in $[Cu_3(\mu\text{-}O)_3]^{2+}$-FER($\mu\text{-}O_2$) with different spin multiplicities

To qualitatively discuss the stability of the active site, it is expressed by Equation 1 as $[Cu(\mu\text{-}O)M]^{2+}$ -FER (M=Fe, Co, Ni), where FER_{2Al} indicates FER with two Al atoms in the unit cell.

$$CuM\text{-}FER_{2Al} + 1/2O_2 \rightarrow [Cu(\mu\text{-}O)M]^{2+}\text{-}FER_{2Al} \quad (1)$$

Table S1 The formation energy of $[Cu\ (\mu\text{-}O)M]^{2+}$ under different spin multiplicities

$[Cu(\mu\text{-}O)M]^{2+}$	Spin multiplicity	Ef (eV)
$[Cu(\mu\text{-}O)Fe]^{2+}$	4	-8.36
	6	-8.33
$[Cu(\mu\text{-}O)Co]^{2+}$	3	-6.47
	5	-6.60
$[Cu(\mu\text{-}O)Ni]^{2+}$	2	-4.94
	4	-4.79

Table S2 The structural characteristics of $[Cu(\mu\text{-}O)M]^{2+}$ under different spin multiplicities

$[Cu(\mu\text{-}O)M]^{2+}$	Spin multiplicity	∠Cu-O-M (°)	d(Cu-O) (Å)	d(M-O) (Å)	d(Cu-M) (Å)	d(Al-Al) (Å)
$[Cu(\mu\text{-}O)Fe]^{2+}$	4	89.08	1.791	1.690	2.443	7.188
	6	95.52	1.807	1.728	2.618	7.101
$[Cu(\mu\text{-}O)Co]^{2+}$	3	85.47	1.795	1.680	2.360	7.196
	5	101.77	1.783	1.698	2.701	7.156
$[Cu(\mu\text{-}O)Ni]^{2+}$	2	84.70	1.776	1.682	2.331	7.244
	4	105.56	1.768	1.688	2.752	7.175

Table S3 Important atomic spin density data of RC and RI in the process of methane to methanol catalyzed by $[Cu(\mu\text{-}O)Co]^{2+}$-FER

	Spin multiplicity	ρ(Cu)	ρ(Co)	ρ(O)	ρ(C)	ρ(H)
Reactant	3	-0.118	1.744	0.212	0.001	0.000
Complex	5	0.418	2.598	0.497	0.002	0.000
Radical	3	-0.186	1.201	0.043	0.440	0.015
Intermediate	5	0.237	2.403	0.200	0.432	0.014

Table S4 Important atomic spin density data of RC and RI in the process of methane to methanol catalyzed by $[Cu(\mu\text{-}O)Ni]^{2+}$-FER

	Spin multiplicity	**ρ(Cu)**	**ρ(Ni)**	**ρ(O)**	**ρ(C)**	**ρ(H)**
Reactant	2	-0.002	0.617	0.282	0.002	0.000
Complex	4	0.492	1.513	0.561	0.003	0.000
Radical	2	0.079	-0.076	0.106	0.428	0.010
Intermediate	4	0.300	1.331	0.229	0.434	0.014

Table S5 The *d*-band centers (*dc*) of RC and RI in the process of methane to methanol catalyzed by $[Cu(\mu\text{-}O)M]^{2+}$-FER

	Spin multiplicity	*dc*	
		Reactant Complex	Radical Intermediate
$[Cu(\mu\text{-}O)Fe]^{2+}$	4	-1.858	-1.536
	6	-1.371	-1.432
$[Cu(\mu\text{-}O)Co]^{2+}$	3	-1.597	-1.662
	5	-1.235	-1.381
$[Cu(\mu\text{-}O)Ni]^{2+}$	2	-1.214	-1.252
	4	-1.356	-1.368

Table S6 The spin population and Bader charge value of $[Cu(\mu\text{-}O)M]^{2+}$ under different spin multiplicities

$[Cu(\mu\text{-}O)M]^{2+}$	**Spin multiplicity**	**Spin population(e/Å³)**			**Bader charge(e)**		
		Cu	M	O	Cu	M	O
$[Cu(\mu\text{-}O)Fe]^{2+}$	4	-0.138	2.717	0.157	0.169	-1.182	0.809
	6	0.374	3.645	0.411	0.164	-1.328	0.862
$[Cu(\mu\text{-}O)Co]^{2+}$	3	-0.122	1.751	0.213	0.155	-1.031	0.732
	5	0.420	2.599	0.498	0.103	-1.192	0.827
$[Cu(\mu\text{-}O)Ni]^{2+}$	2	-0.001	0.621	0.279	0.151	-0.923	0.666
	4	0.494	1.513	0.562	0.045	-1.056	0.783

Table S7 The spin population and Bader charge value of $[Cu(\mu\text{-}O)M]^{2+}$ under different spin multiplicities using the HSE06 functional

$[Cu(\mu\text{-}O)M]^{2+}$	Spin multiplicity	Spin population(e/Å³)			Bader charge(e)		
		Cu	M	O	Cu	M	O
$[Cu(\mu\text{-}O)Fe]^{2+}$	4	0.206	2.214	0.073	-1.136	-1.453	1.100
	6	0.112	4.085	0.172	-1.094	-1.401	1.061
$[Cu(\mu\text{-}O)Co]^{2+}$	3	-0.501	2.342	0.092	0.026	-1.182	0.964
	5	1.624	-0.521	0.237	-0.144	-1.451	0.978
$[Cu(\mu\text{-}O)Ni]^{2+}$	2	1.377	0.751	0.208	-0.175	-0.994	0.816
	4	1.659	0.634	0.458	-0.103	-1.187	0.952

To evaluate the stability of the active site, this work referred to the research protocol proposed by Wang et al.[1] Based on the copper ion-exchange zeolite Cu-FER, different active sites in the metal-exchange FER were presented. The formation mode of the point in the high-temperature activation step, where Cu-FER_{1Al} and Cu_2-FER_{2Al} respectively represent the lattice Cu-FER molecular sieves containing one or two aluminum atoms. In particular, since the number of copper cations in the unit cell of the trinuclear site is greater than that of aluminum atoms, the calculation of the formation energy of the trinuclear site needs to introduce Brønsted and the calculation of the formation energy of the trinuclear site needs to introduce Brønsted H_2-FER_{2Al} molecular sieves in the form of acid are available for comparison at the same level as mononuclear and binuclear sites.

$$Cu\text{-}FER_{1Al} + 1/2O_2 \rightarrow [CuO]^{+}\text{-}FER_{1Al} \quad (2)$$

$$Cu_2\text{-}FER_{2Al} + 1/2O_2 \rightarrow [Cu_2(\mu\text{-}O)]^{2+}\text{-}FER_{2Al} \quad (3)$$

$$2/3Cu_2\text{-}FER_{2Al} - 1/2H_2\text{-}FER_2Al + 1/2H_2O + 4/5O_2 \rightarrow [Cu_3(\mu\text{-}O)_3]^{2+}\text{-}FER_{2Al} \quad (4)$$

Table S8 The formation energy of $[Cu_x(\mu\text{-}O)_y]^{n+}$ under different spin multiplicities

$[Cu_x(\mu\text{-}O)_y]^{n+}$	Spin multiplicity	Ef (eV)
$[CuO]^+$	1	-0.46
	3	-0.75
$[Cu_2(\mu\text{-}O)]^{2+}$	1	-2.80
	3	-2.91
$[Cu_3(\mu\text{-}O)_3]^{2+}$	2	-3.93
	4	-3.98

Table S9 The structural characteristics of $[Cu_x(\mu\text{-}O)_y]^{n+}$ under different spin multiplicities

$[Cu_x(\mu\text{-}O)_y]^{n+}$	Spin multiplicity	∠Cu-O-Cu (°)	d(Cu-O) (Å)		d(Cu-Cu) (Å)	d(Al-Al) (Å)
$[Cu(\mu\text{-}O)]^+$	1	—	1.702		—	—
	3	—	1.712		—	—
$[Cu_2(\mu\text{-}O)]^{2+}$	1	83.28	1.751	1.751	2.327	7.235
	3	90.44	1.771	1.771	2.514	7.206
$[Cu_3(\mu\text{-}O)_3]^{2+}$	2	97.03	1.799	1.776	2.678	7.549
		115.44	1.805	1.811	3.058	
		118.00	1.790	1.770	3.052	
	4	89.44	1.797	1.820	2.545	7.480
		122.50	1.839	1.805	3.195	
		113.16	1.805	1.777	2.990	

Table S10 Important atomic spin density data of RC and RI in the process of methane to methanol catalyzed by $[Cu_2(\mu\text{-}O)]^{2+}$-FER

	Spin multiplicity	ρ(Cu)	ρ(O)	ρ(C)	ρ(H)
Reactant	1	0.000,0.000	0.000	0.000	0.000
Complex	3	0.528,0.528	0.564	0.004	0.002
Radical	1	0.001,0.001	0.000	-0.001	0.000
Intermediate	3	0.367,0.367	0.158	0.441	0.009

Table S11 Important atomic spin density data of RC and RI in the process of methane to methanol catalyzed by $[Cu_3(\mu\text{-}O)_3]^{2+}$-FER ($\mu\text{-}O_1$)

	Spin multiplicity	ρ(Cu1)	ρ(Cu2)	ρ(Cu3)	ρ(O1)	ρ(O2)	ρ(O3)	ρ(C)	ρ(H)
Reactant	2	0.023	0.167	0.181	0.027	0.207	0.240	0.001	0.000
Complex	4	0.016	0.500	0.589	0.729	0.327	0.398	0.010	0.000
Radical	2	-0.004	0.467	0.452	0.051	0.286	0.257	0.428	0.009
Intermediate	4	-0.006	0.461	0.462	0.325	0.272	0.303	0.444	0.007

Table S12 Important atomic spin density data of RC and RI in the process of methane to methanol catalyzed by $[Cu_3(\mu\text{-}O)_3]^{2+}$-FER ($\mu\text{-}O_2$)

	Spin multiplicity	ρ(Cu1)	ρ(Cu2)	ρ(Cu3)	ρ(O1)	ρ(O2)	ρ(O3)	ρ(C)	ρ(H)
Reactant	2	0.022	0.170	0.187	0.024	0.205	0.236	0.000	0.000
Complex	4	0.733	0.323	0.401	0.019	0.493	0.596	0.004	0.000
Radical	2	0.399	0.068	0.475	0.264	0.302	0.036	0.435	0.009
Intermediate	4	0.385	0.065	0.497	0.336	0.272	0.249	0.438	0.009

Table S13 Important atomic spin density data of RC and RI in the process of methane to methanol catalyzed by $[Cu_x(\mu\text{-}O)_y]^{n+}$-FER

0	Spin multi-plicity	Spin population(e/Å³)						Bader charge(e)					
		Cu_1	Cu_2	Cu_3	O_1	O_2	O_3	Cu_1	Cu_2	Cu_3	O_1	O_2	O_3
$[CuO]^+$	1	0.026	—	—	0.031	—	—	1.142	—	—	0.494	—	—
	3	0.606	—	—	1.011	—	—	1.026	—	—	0.419	—	—
$[Cu_2(\mu\text{-}O)]^{2+}$	1	0.030	0.030	—	0.000	—	—	0.939	0.939	—	0.787	—	—
	3	0.531	0.531	—	0.562	—	—	0.962	0.962	—	0.732	—	—
$[Cu_3(\mu\text{-}O)_3]^{2+}$	2	0.022	0.169	0.183	0.026	0.208	0.238	1.144	1.079	1.033	0.682	0.743	0.741
	4	0.021	0.486	0.603	0.727	0.324	0.409	1.152	1.049	1.031	0.636	0.755	0.730

Table S14 Important atomic spin density data of RC and RI in the process of methane to methanol catalyzed by $[Cu_x(\mu\text{-}O)_y]^{n+}$-FER using the HSE06 functional

$[Cu_x(\mu\text{-}O)_y]^{n+}$	Spin multiplicity	Spin population(e/Å³)						Bader charge(e)					
		Cu_1	Cu_2	Cu_3	O_1	O_2	O_3	Cu_1	Cu_2	Cu_3	O_1	O_2	O_3
$[CuO]^+$	1	0.559	—	—	0.479	—	—	1.134	—	—	0.492	—	—
	3	0.611	—	—	1.072	—	—	1.095	—	—	0.422	—	—
$[Cu_2(\mu\text{-}O)]^{2+}$	1	0.448	0.448	—	0.000	—	—	1.029	1.030	—	0.853	—	—
	3	0.603	0.603	—	0.552	—	—	1.060	1.061	—	0.813	—	—
$[Cu_3(\mu\text{-}O)_3]^{2+}$	2	0.372	0.563	0.553	0.319	0.333	0.440	1.229	1.164	1.132	0.629	0.821	0.828
	4	0.420	0.642	0.619	0.898	0.438	0.473	1.240	1.137	1.078	0.576	0.819	0.807

Table S15 The *d*-band centers (*d*c) of RC and RI in the process of methane to methanol catalyzed by $[Cu_x(\mu\text{-}O)_y]^{n+}$-FER

	Spin multiplicity	*d*c	
		Reactant Complex	Radical Intermediate
$[CuO]^+$	1	-1.055	-1.424
	3	-1.100	-1.133
$[Cu_2(\mu\text{-}O)]^{2+}$	1	-1.599	-1.763
	3	-1.095	-0.914
$[Cu_3(\mu\text{-}O)_3]^{2+}(\mu\text{-}O_1)$	2	-1.878	-2.395
	4	-1.811	-2.348
$[Cu_3(\mu\text{-}O)_3]^{2+}(\mu\text{-}O_2)$	2	-2.457	-2.416
	4	-2.450	-2.484

References

1. G. Wang, W. Chen, L. Huang, Z. Liu, X. Sun and A. Zheng, *Catalysis Today*, 2019, **338**, 108-116.